

Structure of the Amino Terminus of a Gap Junction Protein

Priscilla E. M. Purnick,* David C. Benjamin,† Vytas K. Verselis,* Thaddeus A. Bargiello,*¹ and Terry L. Dowd‡

*Department of Neuroscience, Albert Einstein College of Medicine, Bronx, New York 10461; †Beirne B. Carter Center for Immunology Research, University of Virginia, Charlottesville, Virginia 22908; and ‡Department of Pediatrics, Montefiore Medical Center, Albert Einstein College of Medicine, Bronx, New York 10467

Received May 11, 2000, and in revised form June 29, 2000

Charged amino acid residues in the amino terminus of gap junction forming proteins (connexins) form part, if not all, of the transjunctional voltage sensor of gap junction channels and play a fundamental role in ion permeation. Results from studies of the voltage dependence of N-terminal mutants predict that residues 1–10 of Group I connexins lie within the channel pore and that the N-terminus forms the channel vestibule by the creation of a turn initiated by the conserved G12 residue. Here we report that intercellular channels containing mutations of G12 in Cx32 to residues that are likely to interfere with flexibility of this locus (G12S, G12Y, and G12V) do not express junctional currents, whereas a connexin containing a proline residue at G12 (Cx32G12P), which is expected to maintain a structure similar to that of the G12 locus, forms nearly wild-type channels. We have solved the structure of an N-terminal peptide of Cx26 (MD-WGTLQSILGGVNK) using ¹H 2D NMR. The peptide contains two structured domains connected by a flexible hinge (domain-hinge-domain motif) that would allow the placement of the amino terminus within the channel pore. Residues 1–10 adopt a helical conformation and line the channel entrance while residues 12–15 form an open turn. Overall, there is good agreement between the structural and dynamic features of the N-terminal peptide provided by NMR and the functional studies of the voltage dependence of channels formed by wild-type and N-terminal mutations. © 2000

Academic Press

Key Words: NMR; atomic resolution structure; ion channels; voltage-dependent gating; connexins; structure–function.

Gap junctions are intercellular channels that are formed by the interaction of two hemichannels, or connexons, expressed in apposed cells. Each hemichannel is composed of six protein subunits, connexins, arranged in a hexagonal pattern around a large central pore (1, 2) that is estimated to be 6–7 Å in radius (3, 4). Connexins are encoded by a gene family of at least 16 members, which have been divided into two groups based on primary amino acid sequence homology (see 5, 6). The accepted membrane topology of connexins identifies four transmembrane segments (TM1–TM4), three intracellular regions including the N-terminus, a cytoplasmic loop (CL)² connecting TM2 with TM3, and the C-terminus. Two extracellular loops, E1 and E2, connect TM1 with TM2 and TM3 with TM4, respectively. Noncovalent interactions among the extracellular loops of two apposed hemichannels lead to the assembly of the complete intercellular channel (7).

Recent electron cryomicroscopy and image analysis of frozen hydrated two-dimensional gap junction channel crystals achieved at better than 7-Å resolution show four α -helical transmembrane segments organized in two concentric rings around the channel axis (8, 9). Two transmembrane segments within each hemichannel appear to contribute to the formation of the channel lining. A bent helix, probably TM2, lines the portion of the channel pore located toward the intercellular gap (9, 10) while a straight helix, probably TM1, lines the portion of the channel pore located toward the cytoplasmic side of the hemichannel (3, 11). The study provided little direct information regarding the structure of the three intracellular domains, as these were either removed to facilitate image analysis (in the case of the C-terminus) or resolved structures could not be ascribed to specific regions of the primary

¹ To whom correspondence should be addressed. Fax: (718) 430-8821. E-mail: bargiell@aecom.yu.edu.

² Abbreviations used: CL, cytoplasmic loop; RMSD, root-mean-square difference.

sequence. In addition, there are few high-resolution structures of membrane proteins because it is difficult to obtain crystals of sufficient quality for X-ray crystallography. The structure of the amino terminus of gap junctions is of particular interest, as it plays a major role in voltage-dependent gating and is a determinant of ion permeation in Cx32 and Cx26 and presumably other Group I connexins (12, 13, Purnick *et al.*, in press, *Biophys. J.*). We have proposed that the inherent flexibility of a conserved glycine residue (G12) in Group I connexins permits the formation of a turn that creates a channel vestibule by positioning the N-terminal amino acids within the channel pore (12, 13). Glycine has the smallest side chain and can assume conformations that would be forbidden by close contacts for other amino acids with bulkier side chains. Therefore, glycine is more flexible than other residues and is often found in areas of backbone that need to move or hinge (14).

In this paper, we show that the substitution of G12 with proline does not perturb the function of the gap junction channel. This finding supports the structural model, as it is known that a proline residue is able to form a turn in a polypeptide chain (14). The model is further supported by the observed failure of channels to express junctional currents when amino acids that are likely to disrupt a turn (Ser, Tyr, and Val) are substituted for G12. We further examine the model by solving the high-resolution structure of a Cx26 N-terminal peptide (MDWGTLQSILGGVNK) by ¹H 2D NMR techniques. The peptide contains two structured domains connected by a flexible hinge that could position the first 10 amino acids within the channel pore.

MATERIALS AND METHODS

Peptide synthesis. The Cx26 N-terminal peptide (MDWGTLQSILGGVNK) was synthesized at the Laboratory for Macromolecular Analysis at Albert Einstein College of Medicine. The synthesis method was by Fmoc chemistry using an Applied Biosystems 430A automated peptide synthesizer (15). The sample was purified by HPLC and confirmed by electron ionization spectrometry. The peptide was dissolved in 150 mM KCl in 10% ²H₂O/90% H₂O (pH 7.0) at a concentration of 4.0 mM with 150 μM 3-(trimethylsilyl)propionic acid as a chemical shift reference.

¹H 2D NMR. All NMR spectra were collected on a Bruker DRX 600-MHz spectrometer at 283 K. Water suppression in all 2D experiments was accomplished with the double gradient echo method of Hwang and Shaka (16). The data were processed and analyzed using nmrDraw (17). All proton resonances were assigned, by standard procedures (18), using DQF-COSY and both short (16 ms) and long (75 ms) mixing time TOCSY experiments, using 512 TPPI (19) phase-cycled *t*1 increments. Proton-proton distance constraints were obtained from a 250-ms mixing time NOESY experiment. Spin diffusion was not expected for a peptide of this size (15 amino acids) nor was any evidence of spin diffusion observed. The intensity of the NOESY cross peaks was classified into very strong (2.5 Å), strong (3.0 Å), medium (4.0 Å), and weak (5.0 Å) ranges by calibration with known intraresidue distances. Irrelevant intraresidue and sequential distance constraints were deleted within the program DYANA (20). Forty initial structural models were calculated by simulated annealing using torsion angle dynamics as implemented in the pro-

TABLE I
Sequence Alignment of Representative Group I Connexins

Connexin	Species	1	11	21
Cx26	Rat	MDWGTLQSIL	GGVNHKSTSI	GK
Cx26	Sheep	MDWSALQITL	GGVNHKSTSI	GK
Cx30	<i>Xenopus</i>	MNWAGLYAIL	SGVNRHSTSI	GR
Cx30	Mouse	MDWGTLHTVI	GGVNHKSTSI	GK
Cx30.3	Mouse	MNWGFLQGLL	SGVNYKSTAL	GR
Cx31	Human	MDWKTALQALL	SGVNYKSTAF	GR
Cx31	<i>gallus</i>	MDWALQITLL	GGVNHKSTSI	GK
Cx31	Mouse	MDWKKLQDLL	SGVNYKSTAF	GR
Cx31.1	Mouse	MNWSVFEGLL	SGVNYKSTAF	GR
Cx32	Rat	MNWTGLYTL	SGVNRHSTSI	GK
Conserved		M W	GVN ST	G

Note. Conserved hydrophobic residues are shaded in gray.

gram DYANA (20). The 20 structures that gave the lowest value for the DYANA target function were refined by a simulated annealing protocol using the program OPAL (21) to give the final 15 structures that best fit the NMR data.

Site-directed mutagenesis, RNA synthesis, and oocyte injection. Site-directed point mutations were constructed by utilizing oligonucleotide primers and the polymerase chain reaction. Mutated fragments were inserted into wild-type Cx32 cloned into the plasmid vector pGEM7zf+ (Promega), using an engineered *Sal*I site upstream of the initiation codon of Cx32 and either one of the two unique restriction sites, *Pst*I or *Eco*O109I, located within the coding region. The DNA segments containing the PCR-based mutations were sequenced in their entirety. RNA was transcribed *in vitro* from linearized plasmid templates as described in Rubin *et al.* (22). For expression of cloned connexins in *Xenopus* oocytes, approximately 50 nl of 1 ng/nl RNA was coinjected with 0.2 pmol/μl of the phosphorothioate antisense oligonucleotide 5'-GGT TTA GTA ATT CCC ATC CTG CCA TGT TTC-3'. This oligonucleotide is complementary to the 5' end of endogenous *Xenopus* Cx38 and blocks all endogenous coupling between oocyte pairs that is attributable to Cx38 within 72 h (22, 23).

Electrophysiological recording of intercellular channels in pairs of *Xenopus* oocytes. Oocytes were devitelinized and paired 12–36 h after RNA injection. Junctional currents were evident within 4–12 h of pairing and were recorded using a dual-voltage clamp with glass electrodes containing 1 M KCl solutions. Coupled oocytes had similar resting potentials that ranged between –30 and –60 mV, depending on the cell pair. Cells were voltage clamped to their resting potential, resulting in a $V_j = 0$ mV. A family of junctional currents was generated by first applying a brief prepulse of ±20 mV (which was used subsequently to normalize junctional currents) and then by applying a transjunctional voltage of ±5–120 mV in steps of 5- or 10-mV increments. Each step applied was followed by an interpulse interval of 90 s. Currents were digitized at two rates, at 256 Hz for 2 s and then 28 Hz for the remaining 28 s, to allow for increased accuracy in measuring initial currents. Initial and steady-state conductances were obtained from the exponential fitting of I_j .

RESULTS

Table I presents a sequence alignment of the first 22 amino acid residues of six members representative of 22 sequenced Group I or β-connexins. In addition to the N-terminal methionine, seven residues (W3, G12, V13,

N14, S17, T18, and G21) are conserved among all Group I connexins. Amino acids at residues 6, 9, 10, and 19 are always hydrophobic whereas those at the remaining 10 positions are generally hydrophilic. Secondary structure analysis algorithms (Chou–Fasman and Garnier–Osguthorpe–Robson) predict that there are favorable conditions for a turn to exist around residue G12 in all Group I connexins. A turn in the vicinity of G12 is also consistent with the results of studies of the voltage dependence of Cx32 and Cx26 channels. (12, 13, 24; Purnick *et al.*, in press, *Biophys. J.*). Thus, it is likely that the structure of the N-terminus is similar in all Group I connexins.

Mutations of the G12 Residue

To further examine the possibility that a turn exists in the vicinity of the G12 residue, this locus in Cx32 was mutated to residues, Val, Tyr, and Ser, that are expected to perturb the flexibility of the N-terminus. Mutations that interfere with the formation of a turn in this region are expected to significantly affect the conductance–voltage relations of the resulting channels since this region contains part, if not all, of the transjunctional voltage sensor and also plays a role in ion permeation. G12V and G12Y are expected to have the greatest functional effect, as the bulk of their side chains should substantially alter the flexibility of the G12 locus, while G12S is expected to have less of an effect (14). Substitution of the glycine with proline at position 12 is expected to maintain the structure and flexibility of the N-terminus (10).

Representative current traces and conductance–voltage relations of heterotypic pairings of Cx32G12P with Cx32 and Cx26 are shown in Fig. 1. A slight asymmetry is apparent in both the initial and steady-state conductance–voltage relations of Cx32G12P/Cx32 junctions (Fig. 1A). Steady-state junctional conductance decreases at high transjunctional voltages of either polarity to a minimal conductance, $G_{\min} \sim 0.3$. The value of G_{\min} is similar to that reported for homotypic Cx32 pairings (12, 23) and is indicative of channel closure to substates by a form of gap junction voltage dependence termed V_j gating (see 24). The initial and steady-state conductance–voltage relations of the heterotypic Cx32G12P/Cx26 are asymmetric (Fig. 1B) like that of the wild-type Cx26/Cx32 heterotypic junction. The initial conductance–voltage relation of the Cx32G12P/Cx26 junction is somewhat steeper than that of the Cx32/Cx26 junction, rectifying fourfold rather than threefold over a ± 120 -mV range of V_j . The voltage dependence of initial currents reflects the rectification of open channel currents (13, 25). Homomeric hemichannels formed by Cx32G12V, G12Y, or G12S do not express junctional currents in either homotypic or

heterotypic pairings with Cx32 and Cx26 when oocytes are injected with 50 nl of 1 ng/nl RNA.

¹H 1D NMR of an N-Terminal Peptide

The ¹H 1D NMR spectra of the Cx26 peptide (MD-WGTLQSLGGVNK) exhibited well-resolved lines and no significant change in linewidth or chemical shift for peptide concentrations ranging from 0.1 to 4.5 mM. This suggests that in the concentration range tested there is no peptide aggregation and that the peptide is monomeric.

Most small peptides in solution are an ensemble of rapidly interconverting conformations (26). Structural information obtained from NMR is a population-weighted average over all conformations in the ensemble. The presence of strong $d_{\alpha N}(i, i + 1)$ NOE connectivities over an extended region of the peptide indicates a significant population of conformers in the extended chain or random coil forms. Consecutive, intense $d_{NN}(i, i + 1)$ NOE connectivities over a range of residues indicate a significant population of conformers containing turns or helices.

Representative ¹H 2D NMR spectra from the NH- α H region as well as from the NH-aliphatic proton region are shown in Fig. 2. A summary of NOEs for the peptide is shown in Fig. 3A. Moderately strong $d_{NN}(i, i + 1)$ NOE connectivities between residues 2–10 are observed. Lower intensity $d_{\beta N}(i, i + 1)$, $d_{\alpha N}(i, i + 3)$, $d_{\alpha\beta}(i, i + 3)$, and $d_{\alpha N}(i, i + 4)$ NOE connectivities are shown for the same residues. Representative, $d_{\alpha N}(i, i + 3)$, and $d_{\alpha N}(i, i + 4)$ NOEs are shown in the NH- α H region of Fig. 2A. This pattern of NOEs indicates a significant population of folded conformers with helical characteristics. In addition, $d_{\alpha N}(i, i + 1)$ NOE connectivities are shown for the same group of residues. This suggests that extended-chain forms are also present in the conformational ensemble. The peptide contains no longer range NOEs from residues 11–15. The last four residues, G12–K15, are characterized by $d_{\alpha N}(i, i + 1)$, $d_{\beta N}(i, i + 1)$, and weaker $d_{NN}(i, i + 2)$ NOE connectivities. A representative NOE connectivity is shown between 13Val γ CH₃–15LysNH in Fig. 2B. This NOE pattern is usually found in turnlike structures. Figure 3B shows the number of meaningful intraresidue, sequential, and medium to long range NOEs found for each residue in the peptide. It can be seen that medium-range NOEs exist along the entire length of the peptide.

Secondary shifts for C α H resonances are consistent with the NOE results (Fig. 3C). The C α H secondary shift is the difference between the C α H chemical shift in a random coil (18) and the measured shift. A group of resonances exhibiting upfield C α H secondary shifts of 0.15–0.6 ppm is indicative of a helical conformation, with the lower values indicating greater flexibility (27).

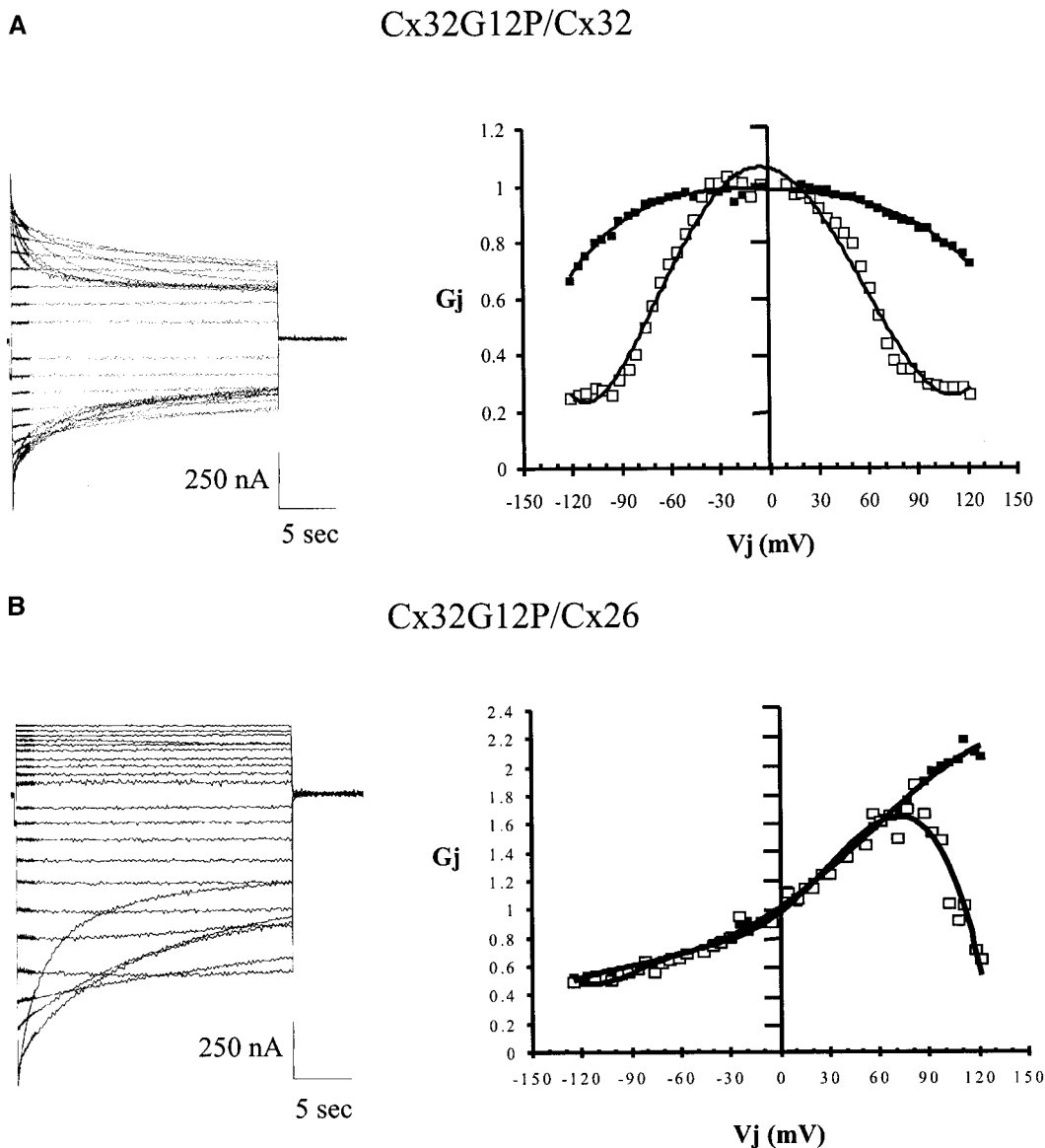


FIG. 1. Conductance–voltage relations and representative traces of junctional currents obtained in pairs of *Xenopus* oocytes. (A) Cx32G12P/Cx32 heterotypic junctions. (B) Cx32G12P/Cx26 heterotypic junctions. V_j corresponds to the voltage applied to the cell expressing the hemichannel appearing on the right side of the channel designation. Filled symbols represent initial conductances and open symbols represent steady-state conductances.

Figure 3C shows that for the Cx26 peptide, secondary shifts for residues 3–7 have values ranging from 0.13 to 0.25, which is indicative of a flexible helical region. The values approach the random coil values for the rest of the peptide, indicating a less structured, more flexible region.

The temperature coefficients are shown for the amide protons in Fig. 3D and are also consistent with the NOE and secondary chemical shift data. The extent to which a temperature coefficient for an amide proton is lowered from the solvent-exposed value of 8×10^{-3} ppm K^{-1} is a measure of the degree

of protection from the solvent and thus of the population of folded conformers (28, 29). Temperature coefficients of less than 6×10^{-3} ppm K^{-1} are suggestive of hydrogen bonding (29). In Fig. 3D the temperature coefficients for the Cx26 peptide show somewhat reduced values of $\sim 6.2 \times 10^{-3}$ ppm K^{-1} for residues G4–S8. This indicates some degree of solvent protection and a population of folded conformers within the population weighted average. A low value of 5×10^{-3} ppm K^{-1} was measured for the amide proton of G12, which suggests that this proton may be involved in a hydrogen bond.

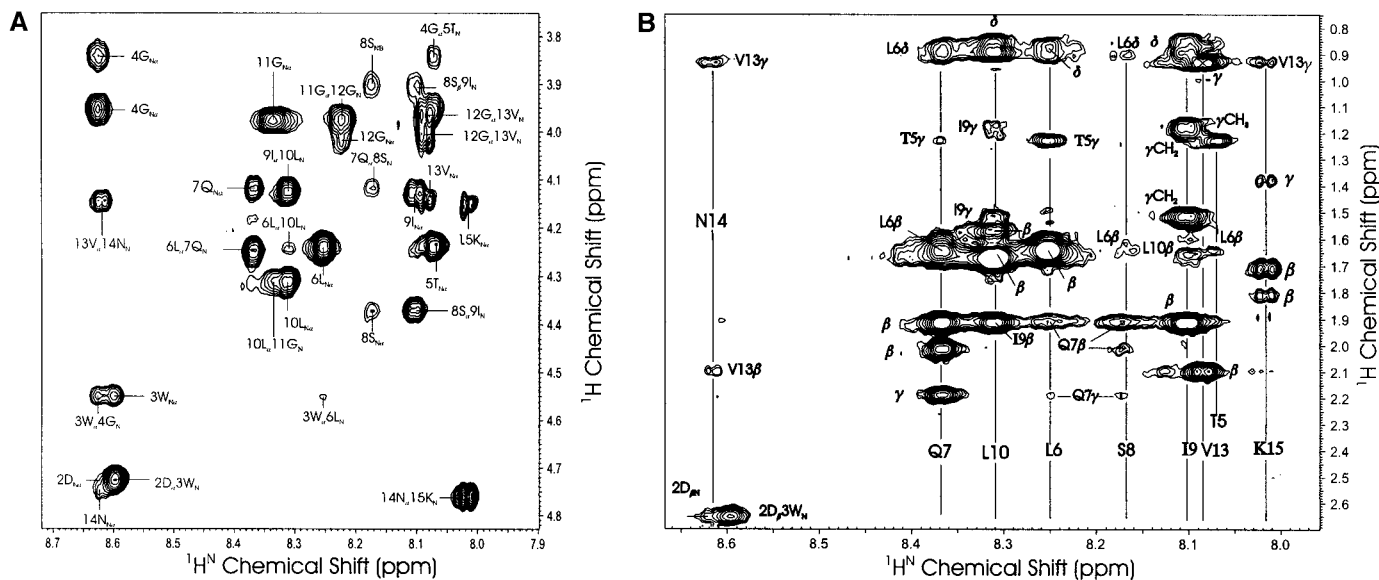


FIG. 2. Sections of the ^1H 2D NOESY spectrum showing the NH- αH region (A) as well as the NH-aliphatic region (B). Representative $d_{\alpha\text{N}}(i, i + 3)$ and $d_{\alpha\text{N}}(i, i + 4)$ NOEs within the helical segment can be seen in A and a representative $13\text{Val}\gamma\text{CH}_3$ - 15LysNH NOE connectivity, found within the C-terminal open turn, can be seen in B.

A total of 92 meaningful distance constraints obtained by the NOESY experiments were used as input to calculate structures with the programs DYANA and OPAL. The structural statistics for the 15 converged structures and atomic root-mean-square differences (RMSDs) are given in Table II. Deviations from idealized covalent geometry are small and the van der Waals energy is negative, indicating no distortions and bad contacts exist in the converged structures. In the Ramachandran plot, the dihedral angles for 95% of all residues in the final 15 converged structures fall in either the most favorable or additionally allowed regions.

The 15 structures that best fit the NMR data are shown in Fig. 4. Superposition of the backbone atoms for residues 1–15 for all structures gives an RMSD value of 1.497 Å (Fig. 4A). The helical characteristics can be observed for residues 2–10; however, the C-terminal end shows turns oriented in different directions which cannot be superimposed for all 15 residues. Superposition of the backbone atoms along residues 1–13 for all 15 structures gives an RMSD of 0.934 Å (Fig. 4B). Again, the helical characteristics can clearly be seen for residues 2–10, with residues 2–6 being more helical and residues 7–10 more flexible. The backbone angles (ϕ , ψ) calculated from the 15 structures deviate from ideal angles defining an α -helix ($\phi = -60^\circ$, $\psi = -60^\circ$). For this reason, we classify the region from residues 2 to 10 as having helical characteristics. A second structural domain is observed when the backbone atoms of residues 11–15 or 12–15 are superimposed. Superposition of residues 11–15 gives an RMSD

value of 0.854 Å (Fig. 4C). G12–K15 form a loose turn, which is not observed when residues 1–15 are superimposed. This indicates that there are two structured domains in the peptide, which are not correlated with each other. There is a turn at the C-terminal end and residues 1–10 maintain the helical characteristics but are not confined to a fixed orientation with respect to the turn. The (ϕ , ψ) backbone angles for residues 12–15 deviate from angles expected for β turns; however, in some of the structures, residues 12–15 do meet the criteria for an open turn since the distance between G12 $\text{C}\alpha$ and K15 $\text{C}\alpha$ is less than 5.7 Å (30).

Side-chain hydrophobic interactions (31, 32), salt bridge formation (33), and hydrogen bonds (29) have been found to stabilize peptide structures. A significant number of NOEs were observed for the Cx26 peptide between side chains of M1 and W3 as well as L6 and W3, indicating close contact. Examination of the structure indicates packing of these hydrophobic amino acid side chains, which could have a stabilizing effect on the helical-like turns. The G12 amide proton was found to have a low temperature coefficient of 5×10^{-3} ppm K^{-1} and a few of the structures show a hydrogen bond acceptor at L10 CO. This may provide some stabilization for the region between L10 and G12 as well as partially stabilize the turn at G12–K15. The open turn at the C-terminus is flexible, with no evidence of hydrogen bonding between K15 NH and G12 CO. Populations of turn conformations are often observed without significant hydrogen bonding (30, 34) and NOEs were observed between V13 and K15 protons (i.e., Figs. 2 and 3B), indicating proximity of these two residues

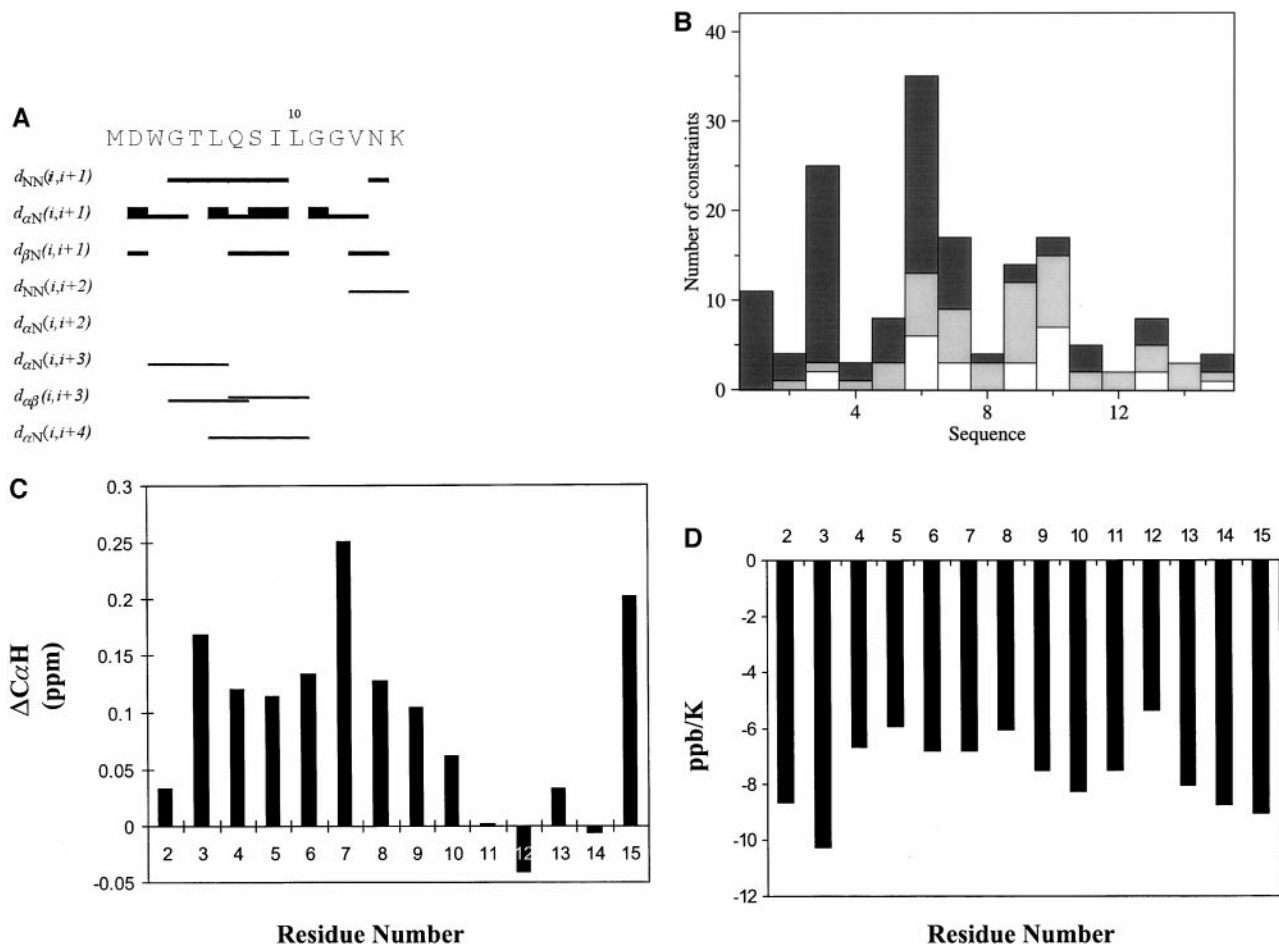


FIG. 3. (A) Diagram summarizing near-neighbor NOEs. The interpretation of the NOEs for secondary structural analysis is given in the text. (B) Number of meaningful intraresidue (white), sequential (light gray), and medium-to-long range (dark gray) NOE constraints per residue. (C) Plot of secondary shifts for the CH_{α} resonance for all residues in the peptide. (D) Plot of temperature coefficients for the NH protons in each residue.

for a significant population of conformers in this conformation.

Molecular Model of the Channel Vestibule

The conformer with the lowest free energy was chosen to create the model of the channel vestibule illustrated in Fig. 5. The chimeric structure was created by combining the structure of the N-terminus of Cx26 solved by NMR (red) and a molecular model of the Cx26 TM1 helix (blue). Six of these structures were arranged to form a model vestibule.

DISCUSSION

We have previously reported that the charge of the second amino acid residue determines the polarity of transjunctional voltage dependence (V_j -gating) of hemichannels formed by Cx32 and Cx26. Based on this and other results, we proposed that this residue lies

within the channel pore, where it can sense the transjunctional electric field (12, 13). In Purnick *et al.* (in press, *Biophys. J*) we report that negative charges of neutral amino acids at the 5th, 8th, 9th, and 10th positions can reverse the polarity of V_j -gating of Cx32 hemichannels, while a negative charge at the 11th residue does not appear to alter V_j -gating polarity. These findings suggest that the first 10 amino acid residues lie within the channel pore. Interestingly, negative charge substitutions of the 8th, 10th, and presumably the 9th residues result in hemichannels that display bipolar V_j -gating; that is, the channels can close in response to either polarity of applied V_j . The simplest explanation for these findings is that the N-terminus of Group I connexins can adopt at least two different open conformations. In one conformation, the 8th, 9th, and 10th residues lie outside the transjunctional electric field, while in another conformation, the first 10 amino acid residues lie within the transjunctional electric field. In this model, residue

TABLE II

Structural statistics	Values for 15 converged structures
Total constraints	92
Intraresidue	23
Sequential	25
Medium range	41
Long range	3
Largest distance constraint violation (Å)	0.37
RMSD	
Backbone (Å)	1.497 (residues 1–15), 0.934 (residues 1–13), 0.854 (residues 11–15)
Heavy atoms (Å)	2.116 (residues 1–15), 1.171 (residues 1–13), 1.756 (residues 11–15)
Deviations from idealized geometry	
Bonds (Å)	0.007 ± 0.0008
Angles (deg)	2.14 ± 0.23
van der Waals energy (kcal/mol)	–31.41

11 and more upstream residues would always lie outside the field, as would be expected if the N-terminal segment contained a turn in this region.

The central feature of the proposed structural model is that the inherent flexibility provided by the G12 residue would result in the formation of a turn that positions the N-terminus within the channel pore. The outcome of the mutational studies of the G12 residue supports this hypothesis. Substitutions of the G12 residue with amino acids, which are expected to reduce the flexibility of the locus (Ser, Val, and Tyr), do not allow the expression of junctional currents, whereas the proline substitution, which is often found in turns and is expected to maintain the flexibility of the hinge region, forms intercellular channels that are characterized by nearly wild-type voltage dependence. This result suggests that the structure–function relation of the N-terminus is not substantially perturbed by the G12P mutation. The increase in rectification of initial conductance of the heterotypic Cx32G12P/Cx26 junction can be explained by a change in the position of the positively charged N-terminal methionine residue in the transjunctional electric field (see 13).

The NMR data show that both residue 2 and residue 5 lie within the stable helical region and that residues 8–10 are located within the less stable helical region closer to the flexible hinge. Figure 5 illustrates how these residues may be positioned within the transjunctional electric field by the domain–hinge–domain motif that is adopted by the Cx26 peptide. A similar domain–hinge–domain motif has been observed for antimicrobial peptides as well (35, 36). In the sacrotoxin IA peptide (36), the flexibility between the two domains is

due to the presence of glycine residues. A recent NMR study of an isolated sodium channel inactivation gate peptide (37) demonstrates that the peptide forms a stable helical structure capped by an N-terminal turn in H₂O. Unstructured glycine- and proline-rich regions flank the folded core of the peptide, which is consistent with their proposed role as hinges in intact channels.

The wide range of dynamic structural conformations (flexibility) evident in the NMR spectra of the Cx26 peptide hinge region might allow amino acids 8–10 to lie either in or out of the electric field and thereby could account for the presence of at least two open-channel states. These multiple states might also result from more “global” conformational changes that would alter the radius of the channel pore (see Purnick *et al.*, in press, *Biophys. J.*). The intrinsic flexibility of the N-terminus may also explain the brief (1.5 ms) duration channel closures reported by Oh *et al.* (24). These closures may be a result of a partial movement of the N-terminal amino acids in and out of the electric field or could be due to the rotational flexibility of the hinge region about its helical axis.

For the most part, the model depicted in Fig. 5 illustrates how the first eight amino acids could lie in the transjunctional electric field. While the conformer shown in Fig. 5 is the one with lowest free energy in a 100 mM KCl solution, other conformers exist which adopt a structure that would place the 11th residue outside the channel vestibule while keeping the first 10 residues within the channel pore.

The Cx32G12S mutation is one of more than 100 Cx32 loss-of-function mutations that cause the X-linked form of a hereditary neuropathy, Charcot–Marie–Tooth disease (see 38). We report in this study that substitutions of the G12 residue in Cx32 with amino acids that are expected to reduce the flexibility of the locus (Ser, Val, and Tyr) do not express junctional currents. Deschenes *et al.* (39) have suggested that the absence of the Cx32G12S expression at the cell surface may be the result of improper membrane insertion. If G12 were part of a signal sequence contained in the N-terminus required for proper membrane insertion, then all substitutions might be expected to disrupt targeting of Cx32 to the membrane, irrespective of the functional attributes of the amino acid residues. Our results suggest that ability of mutations to express junctional currents is related to the bulk and flexibility of the 12th residue. Furthermore, only 7 out of 22 N-terminal residues are conserved in Group 1 connexins (Table I), suggesting that if a signal sequence exists, it is highly degenerate. The existence of an N-terminal specific signal sequence is not supported by the robust expression of junctional currents that is observed for Cx32 mutations at the 2nd, 5th, and 8th positions (Purnick *et al.*, in press, *Biophys. J.*). We suggest that N-terminal mutations that do not express

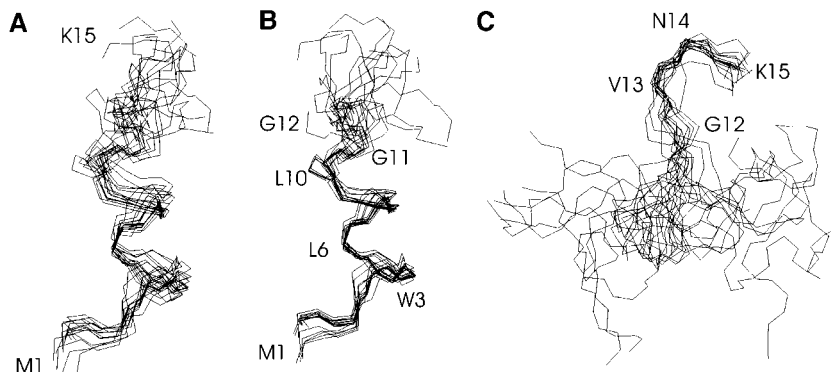


FIG. 4. Structure of the Cx26 peptide. Superposition of the backbone atoms for the 15 lowest energy structures is shown. Superposition of the backbone atoms for residues 1–15 is shown in A, 1–13 in B, and 11–15 in C.

junctional currents may alter the conformation of this region of the protein. This change in conformation may interfere with membrane targeting or insertion by a mechanism unrelated to the action of a signal se-

quence. Alternatively, these mutations may allow the insertion of a hemichannel, which preferentially adopts a closed conformation channel, into the membrane.

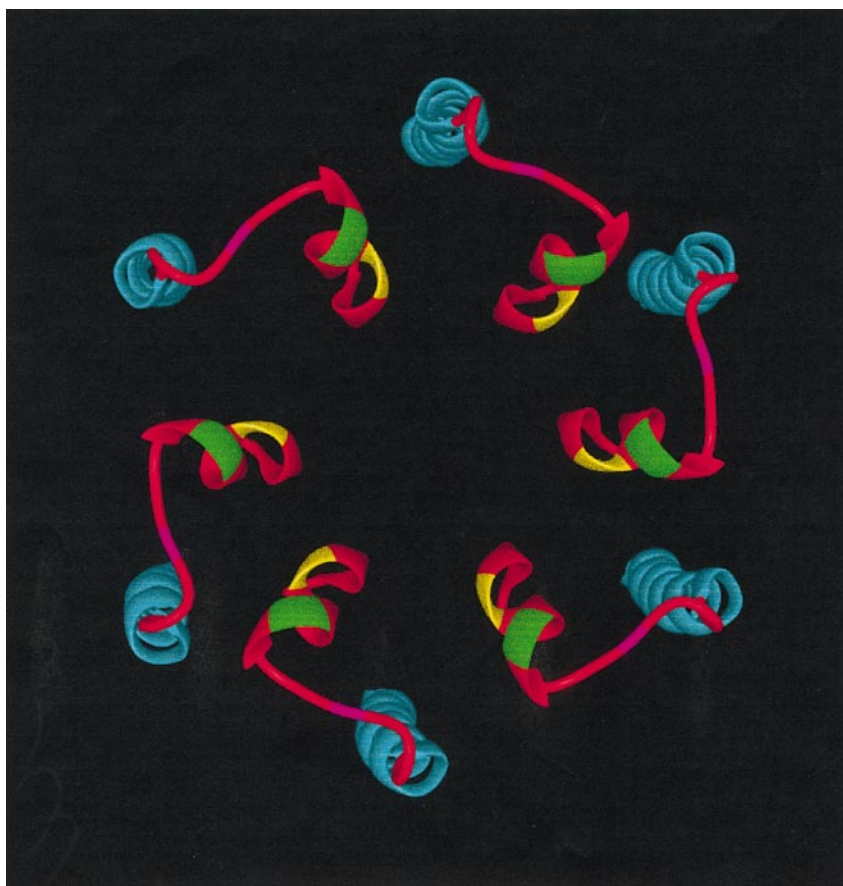


FIG. 5. Molecular model of a portion of a Cx26 hemichannel viewed from the cytoplasmic face. The structure contains the NMR-derived structure of the first 15 amino acids of Cx26 attached to residues 16–42 (blue), which includes the first transmembrane domain. This figure shows the axial projection viewed from the cytoplasmic surface of six subunits forming the channel vestibule. The conserved glycine residue (G12) is shaded violet, the fifth residue is shaded yellow, and the eighth residue is shaded green. The helix formed by residues 2–10 forms the channel vestibule.

It is interesting to note that, in addition to G12S, the mutations W3R and W3S result in CMT. The NMR structure of the Cx26 peptide indicates that residues M1, W3, and L6 are in close contact and it is likely that the packing of these conserved hydrophobic residues stabilizes the helical character of this portion of the N-terminus. When mutated to a negative charge, Cx32W3D does not express junctional currents. We suggest that the polar nature of the W3 CMT mutations may impair the stabilization of the helix that is due to the packing of the hydrophobic residues and may cause a conformational change that results in CMT (3).

Other mutations, V13M, N14K, R15Q,W, and H16P, are known to result in CMT. The structure derived from the NMR analysis of the closely related Cx26 peptide indicates that residues G12–K15 form an open turn and it is likely that CMTX mutations of residues 12–15 alter the structure of this turn or impair its flexibility. While we have not examined the voltage dependence of all mutations in this region, intercellular channels formed by R15Q and R15W exhibit large shifts in their steady-state conductance–voltage relations, suggesting that they have a preference for the closed conformation at voltages at which the wild-type channel would be open (C. K. Abrams, personal communication). Another negative-charge substitution, Cx32L6D, also does not express junction currents, perhaps by disrupting the hydrophobic packing of the N-terminal region of the helix described above.

This paper shows that the N-terminal segment of Cx26 has a defined structure in the absence of the transmembrane helix and the membrane. While it is likely that the structure of the N-terminus of Cx26 may be influenced by interactions with other domains, notably the cytoplasmic loop (13) and regions of the first transmembrane domain, both the biophysical and structural studies that are described in this paper and in Purnick *et al.* (in press, *Biophys. J.*), Verselis *et al.* (12), and Oh *et al.* (13) indicate that the NMR-derived solution structure of the Cx26 N-terminal peptide is likely to be quite similar to its conformation in the native channel. This result is perhaps not surprising as the amino terminus of the native channel is expected to reside in an aqueous environment similar to that used in the determination of the NMR spectra. The exact length of the N-terminal segment in the cytoplasm is not known. A study of Cx32 from isolated intact liver gap junctions demonstrated that residues 7–11 were accessible to cleavage by proteinase A. (40). This result is consistent with a structural model that places these residues at or near the cytoplasmic surface of the gap junction channel. It is thought that membrane proteins extend from the membrane at amino acids with positively charged side chains, since these side chains could serve as anchors to the membrane. In the N-terminus of connexin proteins, these amino acids are

located at positions 15 and 22. Lysine (residue 15) is the C-terminus of the peptide in this study and it may be that this is the shortest possible N-terminal segment extending into the cytoplasm. The structure of the cytoplasmic loop of another transmembrane protein, rhodopsin, used similar NMR methods on a peptide comprising 22 amino acid residues of the third cytoplasmic loop and obtained a defined structure for residues 7–22 (41). Our results suggest that high-resolution NMR-derived structures of isolated peptides in conjunction with biophysical and molecular genetic studies may be valuable in determining the structure of protein domains that are not readily solved by other means.

ACKNOWLEDGMENTS

We thank Drs. M. Girvin, S. Cahill, and S. Almo for helpful discussions and Dr. M. Bennett for comments on the manuscript. This work was supported by NIH Grant GM46889 to T.A.B. and ES09032 to T.L.D. P.E.M.P. was supported by a NIH predoctoral training grant (DK07513).

REFERENCES

1. Unwin, P. N., and Zampighi, G. (1980) *Nature* **283**, 545–549.
2. Makowski, L., Caspar, D. L., Phillips, W. C., and Goodenough, D. A. (1977) *J. Cell Biol.* **74**, 629–645.
3. Oh, S., Ri, Y., Bennett, M. V. L., Trexler, E. B., Verselis, V. K., and Bargiello, T. A. (1997) *Neuron* **19**, 927–938.
4. Beblo, D. A., and Veenstra, R. D. (1997) *J. Gen. Physiol.* **109**, 509–522.
5. Bennett, M. V. L., Zheng, X., and Sogin, M. L. (1994) *Soc. Gen. Physiol. Ser.* **49**, 223–233.
6. Kumar, N. M., and Gilula, N. B. (1996) *Cell* **84**, 381–388.
7. Ghoshroy, S., Goodenough, D. A., and Sosinsky, G. E. (1995) *J. Membr. Biol.* **46**, 15–28.
8. Unger, V. M., Kumar, N. M., Gilula, N. B., and Yeager, M. (1997) *Nat. Struct. Biol.* **4**, 39–43.
9. Unger, V. M., Kumar, N. M., Gilula, N. B., and Yeager, M. (1999) *Science* **283**, 176–1180.
10. Ri, Y., Ballesteros, J. A., Abrams, C. K., Oh, S., Verselis, V. K., Weinstein, H., and Bargiello, T. A. (1999) *Biophys. J.* **76**, 2887–2898.
11. Zhou, X. W., Pfahnl, A., Werner, R., Hudder, A., Llanes, A., Luebke, A., and Dahl, G. (1997) *Biophys. J.* **72**, 1946–1953.
12. Verselis, V. K., Ginter, C. S., and Bargiello, T. A. (1994) *Nature* **368**, 348–351.
13. Oh, S., Rubin, J. B., Bennett, M. V. L., Verselis, V. K., and Bargiello, T. A. (1999) *J. Gen. Physiol.* **114**, 339–364.
14. Richardson, J. S. (1981) *Adv. Protein Chem.* **34**, 167–339.
15. Angelleti, R. H., Mints, L., Aber, C., and Russell, J. (1996) *Endocrinology* **137**, 2918–2922.
16. Hwang, T. L., and Shaka, A. J. (1998) *J. Magn. Reson.* **135**, 280–287.
17. Delaglio, F., Grzesiek, S., Vuister, G. W., Zhu, G., Pfeifer, J., and Bax, A. (1995) *J. Biomol. NMR* **6**, 277–293.
18. Wüthrich, K. (1986) *NMR of Proteins and Nucleic Acids*, Wiley, New York.
19. Marion, D., and Wüthrich, K. (1983) *Biochem. Biophys. Res. Commun.* **113**, 967–974.

20. Guntert, P., Mumenthaler, C., and Wüthrich, K. (1997) *J. Mol. Biol.* **273**, 283–298.
21. Luginbühl, P., Guntert, P., Billeter, M., and Wüthrich, K. (1996) *J. Biomol. NMR* **8**, 136–146.
22. Rubin, J. B., Verselis, V. K., Bennett, M. V. L., and Bargiello, T. A. (1992) *Biophys. J.* **62**, 183–195.
23. Barrio, L. C., Suchyna, T., Bargiello, T. A., Xu, L. X., Roginski, R. S., Bennett, M. V. L., and Nicholson, B. J. (1991) *Proc. Natl. Acad. Sci. USA* **88**, 8410–8414.
24. Oh, S., Abrams, C. K., Verselis, V. K., and Bargiello, T. A. (2000) *J. Gen. Physiol.* **13**, 13–31.
25. Bukauskas, F. F., Elfgang, C., Willecke, K., and Weingart, R. (1995) *Pflügers Arch.* **429**, 870–872.
26. Dyson, H. J., and Wright, P. E. (1991) *Annu. Rev. Biophys. Biophys. Chem.* **20**, 519–538.
27. Wishart, D. S., Sykes, B. D., and Richards, F. M. (1991) *J. Mol. Biol.* **222**, 311–333.
28. Dyson, H. J., Satterthwait, A. C., Lerner, R. A., and Wright, P. E. (1990) *Biochemistry* **29**, 7828–7837.
29. Dyson, H. J., Rance, M., Houghten, R. A., Lerner, R. A., and Wright, P. E. (1988) *J. Mol. Biol.* **201**, 161–200.
30. Crawford, J. L., Lipscomb, W. N., and Schellman, C. G. (1973) *Proc. Natl. Acad. Sci. USA* **70**, 538–542.
31. Dadlez, M., Bierzynski, A., Godzik, A., Sobocinska, M., and Kupryszewski, G. (1988) *Biophys. Chem.* **31**, 175–181.
32. Wang, G., Pierens, G. K., Treleaven, W. D., Sparrow, J. T., and Cushley, R. J. (1996) *Biochemistry* **35**, 10358–10366.
33. Rico, M., Gallego, E., Santoro, J., Bermejo, F. J., Nieto, J. L., and Herranz, J. (1984) *Biochem. Biophys. Res. Commun.* **123**, 757–763.
34. Lewis, P. N., Momany, F. A., and Scheraga, H. A. (1973) *Biochim. Biophys. Acta* **303**, 211–229.
35. Wong, H., Bowie, J. H., and Carver, J. A. (1997) *Eur. J. Biochem.* **247**, 545–557.
36. Iwai, H., Nakajima, Y., Natori, S., Arata, Y., and Shimada, I. (1993) *Eur. J. Biochem.* **217**, 639–644.
37. Rohl, C. A., Boeckman, F. A., Baker, C., Scheuer, T., Catterall, W. A., and Klewit, R. E. (1999) *Biochemistry* **38**, 855–861.
38. Scherer, S. S. (1997) *Neuron* **18**, 13–16.
39. Deschenes, S. M., Walcott, J. L., Wexler, T. L., Scherer, S. S., and Fischbeck, K. H. (1997) *J. Neurosci.* **17**, 9077–9084.
40. Hertzberg, E. L., Disher, R. M., Tiller, A. A., Zhou, Y., and Cook, R. G. (1988) *J. Biol. Chem.* **35**, 19105–19111.
41. Yeagle, P. L., Alderfer, J. L., and Albert, A. D. (1995) *Biochemistry* **34**, 14621–14625.